

# A Geometric Computational Model for Calculation of Longwall Face Effect on Gate Roadways

Hamid Mohammadi<sup>1</sup> · Mohammad Ali Ebrahimi Farsangi<sup>1</sup> · Hossein Jalalifar<sup>1</sup> · Ali Reza Ahmadi<sup>2</sup>

Received: 5 October 2014 / Accepted: 14 March 2015 / Published online: 20 March 2015  
© Springer-Verlag Wien 2015

**Abstract** In this paper a geometric computational model (GCM) has been developed for calculating the effect of longwall face on the extension of excavation-damaged zone (EDZ) above the gate roadways (main and tail gates), considering the advance longwall mining method. In this model, the stability of gate roadways are investigated based on loading effects due to EDZ and caving zone (CZ) above the longwall face, which can extend the EDZ size. The structure of GCM depends on four important factors: (1) geomechanical properties of hanging wall, (2) dip and thickness of coal seam, (3) CZ characteristics, and (4) pillar width. The investigations demonstrated that the extension of EDZ is a function of pillar width. Considering the effect of pillar width, new mathematical relationships were presented to calculate the face influence coefficient and characteristics of extended EDZ. Furthermore, taking GCM into account, a computational algorithm for stability analysis of gate roadways was suggested. Validation was carried out through instrumentation and monitoring results of a longwall face at Parvade-2 coal mine in Tabas, Iran, demonstrating good agreement between the new model and measured results. Finally, a sensitivity analysis was carried out on the effect of pillar width, bearing capacity of support system and coal seam dip.

**Keywords** Gate roadway · Excavation-damaged zone (EDZ) · Longwall face · Caving zone (CZ) · Geometric computational model (GCM)

## List of symbols

$a_i$	Half of the EDZ width
$A_iB_iC_i$	Triangular damaged zone
$A_iG_i$	Dimension parameter
$A_iH_i$	Dimension parameter
$B_{Gi}$	Gate roadway width
$B_{ni}$	EDZ height
$B_{ni,ext}$	Height of extended EDZ
$d$	Expansion factor of broken rock
$D_iG_i$	Dimension parameter
$f_1'(x)$	Computational function
$f_1''(x)$	Computational function
$f_2'(x)$	Computational function
$f_2''(x)$	Computational function
$F_iG_i$	Dimension parameter
$F_iH_i$	Dimension parameter
$H_i$	Gate roadway depth from the ground level
$H_{E,i}$	Equivalent height of overburden
$H_C$	CZ height
$h_i$	Gate roadway height
$h_{p,i}$	Pillar height
$h_{\Delta i}$	Height of triangle $A_iB_iC_i$
$h_s$	Coal seam thickness or face height
$J_i$	Vertical distance between pillar and the roof of gate roadway
$L$	Face length
$FIC_i$	Face influence coefficient
$q_i$	Bearing capacity of the support system
$S_{add,i}$	Area of the extended part of EDZ
$S_{ext,i}$	Area of the extended EDZ (total area of EDZ)
$S_{par,i}$	Parabolic area of EDZ

✉ Hamid Mohammadi  
mohammadi\_79@yahoo.com

<sup>1</sup> Mining Engineering Department, Shahid Bahonar University of Kerman, Kerman, Iran

<sup>2</sup> Mechanical Engineering Department, Graduate University of Advanced Technology, Kerman, Iran

$S_{\Delta_i}$	Area of triangle $A_iB_iC_i$
$S \cdot F_i$	Safety factor
$u_i$	Roof displacement
$u_{i,\text{ext}}$	Total roof displacement
$W_i$	Pillar width
$x'_1$	Boundary of integration
$x'_2$	Boundary of integration
$x''_1$	Boundary of integration
$x''_2$	Boundary of integration
$L_i$	Pillar length

### Greek symbols

$A$	Coal seam dip angle
$\beta_i$	Influence angle of CZ
$\gamma$	Unit weight of rock mass
$\sigma_{0i}$	Vertical in situ stress
$\sigma_c$	Uniaxial compressive strength of a cubical specimen
$\sigma_{cm}$	Compressive strength of materials
$\sigma_i$	Average pillar stress
$\sigma_{pi}$	Pillar strength
$\phi_i$	Average angle of shear of roof strata
$\phi_{0i}$	Caving angle
$\phi_p$	Peak internal friction angle of rock mass

### Subscript

$i$  Defines gate roadways, i.e.,  $i = 1$  is for the main gate roadway and  $i = 2$  represents the tail gate roadway

## 1 Introduction

In advance longwall mining, the stability of the main gate and tail gate roadways plays an important role in the safety of mine network, production rate, and consequently the economic condition (Yavuz 2004; Lawrence 2009; Jiao et al. 2013). The gate roadway stability is a function of two important factors: (1) characteristics of the excavation-damaged zone (EDZ) above the gate roadway and (2) the longwall face effect (Unal et al. 2001; Torano et al. 2002; RafiqulIslam et al. 2009; Gao et al. 2014a). EDZ is a non-elastic zone with geomechanical modifications, inducing significant changes in resistance properties and behavior of rock mass, which are created during construction of the gate roadway (Pusch and Stanfors 1992; Chang et al. 2007).

It should be noted that, in advance longwall mining, EDZ is expandable because of additional loadings due to face effect. In reality, after advancing the face support system, a null space is created behind the support system and its immediate roof. In such situation, the immediate roof collapses and caves. Due to downward movement of roof strata, a caving zone (CZ) with height of  $H_C$  above the face is created. Consequently, the overburden pressure

above CZ is redirected toward the face and both sides where gate roadways are located. In fact, the overburden pressure above CZ produces an additional loading on the gate roadways, which causes an extension in EDZ (Yavuz 2004; Lawrence 2009; Snuparek and Konecny 2010; Mohammadi et al. 2013).

Different methods such as numerical modeling, physical modeling, analytical solution, and empirical methods have been developed to determine the effect of longwall face on the gate roadway stability (Whittaker and Singh 1981; Shen et al. 2003; Lin and Zhang 2011). Considering the horizontal longwall face along with instrumentation and monitoring results of some main gate roadways, it has been shown that the face effect on gate roadways can be determined from geometric concept of the longwall mining mechanism (Snuparek and Konecny 2010). Based on this concept, due to face effect, a triangular damaged zone is created above the main gate roadway and the additional loading is related to the extended part of EDZ, which is equal to the difference between the triangular zone area and the EDZ area (Mohammadi et al. 2013). However, a study of previous geometric models shows that there are some major shortcomings as follows:

(1) EDZ properties have been obtained using simple empirical relationships with no regard to the ratio of in situ stress and uniaxial strength of the rock mass. (2) Models are based on horizontal longwall face, whereas the majority of longwall faces are inclined. (3) All relationships for modeling the effect of face on EDZ are approximated with low accuracy. (4) Models only consider the main gate roadway, and the tail gate roadway stability is not included.

In this paper, a geometric computational model (GCM) has been developed to calculate the effect of longwall face on the extension of EDZ above the gate roadways without the mentioned shortcomings. To this end, first, new empirical relations are presented for calculating the EDZ properties. Second, considering the pillar width effect and coal seam properties, GCM is designed to calculate the characteristics of extended EDZ. Third, a new mathematical formulation is presented to determine the face influence coefficient, and finally a computational algorithm is suggested to analyze the gate roadways stability.

## 2 EDZ Characteristics Without the Face Effect

Characteristics of EDZ are dependent on geomechanical properties of the rock mass, depth, size, and shape of the gate roadway. The shape of the gate roadway plays an important role in achieving long-term stability. Despite applicability of rectangular cross section, a large number of coal mining gate roadways are arch shaped supported by steel girders (Jukes 1985; Torano et al. 2002; Horyl and

Marsalek 2014). A wide variety of methods have been developed to assess the EDZ characteristics, such as instrumentation and monitoring, laboratory physical simulation, numerical modeling, and empirical methods (Biron and Arioglu 1983; Pariseau 2007; Snuparek and Konecny 2010; Lin and Zhang 2011). One of the empirical methods is arch theory. Based on this theory, during the construction of gate roadway, EDZ may be produced as a natural arch as the resistance properties of the rock mass is decreased. Rocks will loosen and separate from the upper part of the overburden along the arch (Pariseau 2007). Figure 1 shows a schematic view of EDZ above the main gate and tail gate roadways before coal mining. In this figure,  $H_i$  is the gate roadway depth as measured from the ground level,  $B_{Gi}$  is the gate roadway width,  $h_i$  is the gate roadway height,  $B_{ni}$  is the EDZ height,  $a_i$  is half of the EDZ width,  $\alpha$  is the coal seam dip angle, and  $\varphi_p$  is the peak internal friction angle of the rock mass. Subscript  $i$  defines gate roadways, i.e.,  $i = 1$  is for the main gate roadway and  $i = 2$  represents the tail gate roadway.

Janas, while considering the arch theory and utilizing the instrumentation and monitoring results of gate roadways in Ostrava-Karviná coalfield (OKR), presented two empirical relationships for calculating the roof displacement and height of EDZ as follows (Janas 1990; Janas et al. 2009; Snuparek and Konecny 2010):

$$u_i = 0.1B_{Gi} \left( e^{\frac{1.5H_i - q_i}{45\sigma_{cm}}} - 1 \right), \tag{1}$$

$$B_{ni} = 2B_{Gi} \left( e^{0.03\frac{H_i}{\sigma_{cm}}} - 1 \right)^{0.6}, \tag{2}$$

where  $u_i$  is the roof displacement of the gate roadway (m),  $\sigma_{cm}$  is the compressive strength of materials above the gate roadway (MPa), and  $q_i$  is the bearing capacity of the support system at the gate roadway (kPa).

In Eqs. (1) and (2), the ratio of in situ stress to compressive strength of materials has not been considered, whereas Hoek (1998) showed that if the rock mass strength falls below 20 % of in situ stress in no support condition, the EDZ size increases rapidly and control of stability condition becomes difficult. Therefore, the Janas method was checked against the results from instrumentation and monitoring of gate roadways at Parvade-2 coal mine in Tabas with different cross sections such as arch shaped, rectangular, and trapezoidal sections. Studies have shown that since in Janas method the ratio between in situ stress and uniaxial compressive strength of rock mass is not considered, the accuracy of this method is not high; therefore, taking into account the instrumentation and monitoring results, the Janas relationships have been modified as follows:

$$u_i = 0.1B_{Gi} \left( e^{\frac{\sigma_{0i} - \gamma q_i}{\sigma_{cm}}} - 1 \right), \tag{3}$$

$$B_{ni} = 2.08B_{Gi} \left( e^{\frac{\sigma_{0i}}{\sigma_{cm}}} - 1 \right)^{0.6}, \tag{4}$$

where,  $\sigma_{0i}$  is the vertical in situ stress at the gate roadway roof (MPa) and  $\gamma$  is the unit weight of the rock mass (MN/m<sup>3</sup>).

### 3 Modeling Face Effect on Gate Roadways

Due to advancing coal face, a CZ above the longwall face is created and the stress field is redistributed; consequently, a triangular damaged zone is created above the gate roadway and an additional loading is applied to coal pillars and EDZ, which causes an extension in EDZ. To calculate the face effect on EDZ of gate roadways, GCM is presented as in Fig. 2. As shown in this model, contrary to previous

**Fig. 1** EDZ characteristics of the main gate and tail gate roadways before coal extraction by advance longwall mining

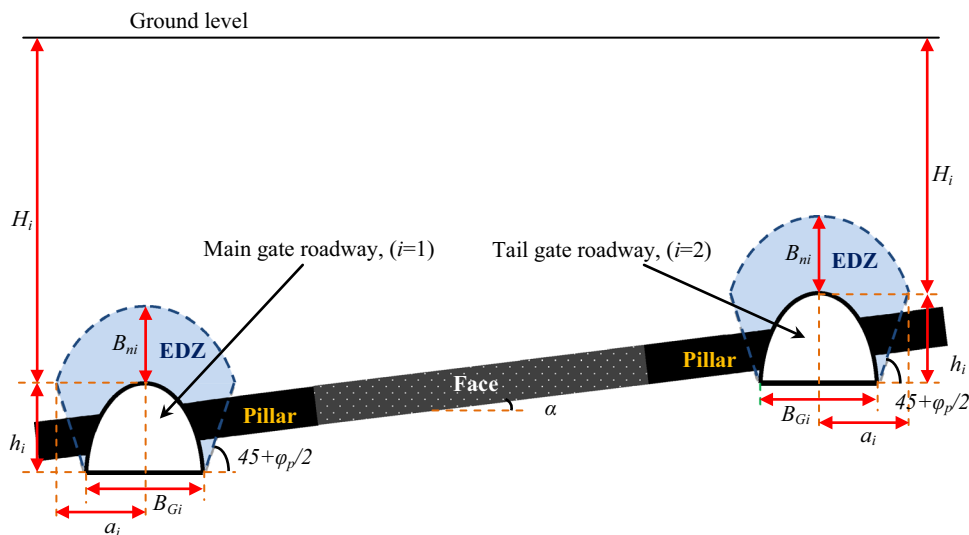
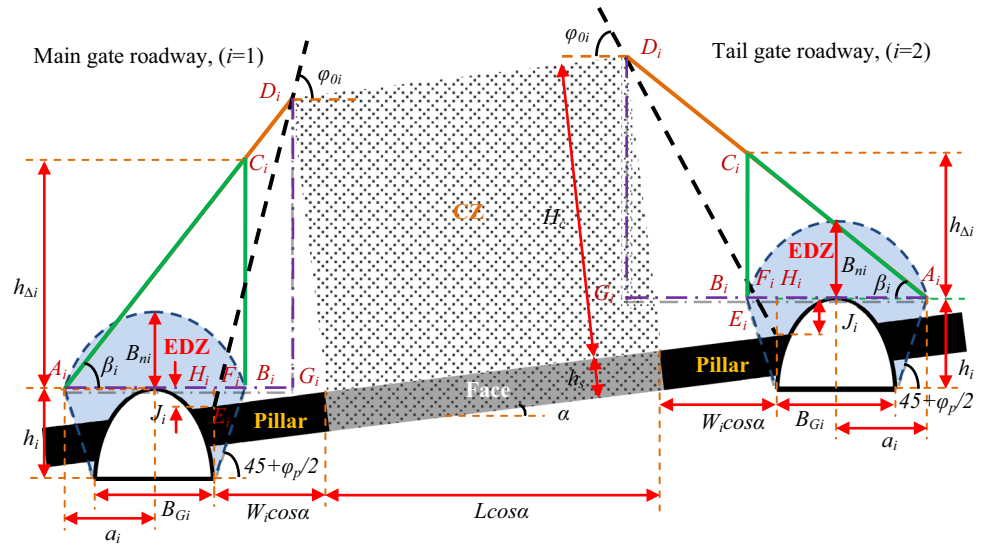


**Fig. 2** GCM to determine the face effect on the main gate and tail gate roadways considering advance longwall mining



models, four important subjects are considered: (1) coal seam dip, (2) vertical distance between the coal pillar and the roof of the gate roadway (it determines the coal seam location at the sidewall of the gate roadway), (3) stability condition of the tail gate roadway, and (4) different gate roadway cross sections. According to GCM, the damaged zone is the triangle  $A_iB_iC_i$  and additional loading relates to the part of triangle  $A_iB_iC_i$  located outside the parabolic area of EDZ. In Fig. 2,  $h_s$  is the coal seam thickness or face height,  $\varphi_{0i}$  is the caving angle,  $\beta_i$  is the influence angle of CZ,  $W_i$  is the pillar width,  $J_i$  is the vertical distance between pillar and the roof of gate roadway,  $L$  is the face length, and  $h_{\Delta i}$  is the height of triangle  $A_iB_iC_i$ .

To influence coal mining operation within the face on gate roadways, the level of the upper interface between CZ and overburden must be higher than the level of the gate roadway roof; hence, Eqs. (5) and (6) must be satisfied for the main gate and tail gate roadways, respectively:

$$H_C \cos \alpha + W_1 \sin \alpha > J_1, \tag{5}$$

$$H_C \cos \alpha > J_2 + W_2 \sin \alpha. \tag{6}$$

The height of triangle  $A_iB_iC_i$  depends on the height of CZ. To calculate the area of this triangle, CZ height must be calculated first. Many researchers have investigated CZ characteristics (Chuen 1979; Singh and Kendorski 1981; Peng and Chiang 1984; Fawcett et al. 1986; Zhou 1991; Suchowerska et al. 2012; Gao et al. 2014b). Recently, a study was carried out on the relation between CZ shape and CZ height (Majdi et al. 2012). In this study, it was shown that there were two general models for CZ: (1) geometry-independent roof fracture and (2) geometry-dependent roof fracture. Considering these general models along with results from in situ measurements, five mathematical models

were presented to calculate the CZ height. One of these models is an arithmetic model, which is a sub-model of the geometry-independent roof fracture model. Based on this model, tensile failure occurs at two extreme ends of the panel perpendicular to the advancing direction. Hence, the width of the CZ is equal to the extracted panel width. Moreover, it was shown that in this model, the CZ height is a nonlinear function of two parameters, namely, the coal seam thickness and the expansion factor of broken rock within CZ ( $d$ ), and includes the Peng model as well (Majdi et al. 2012). In this research, the CZ height is calculated based on the arithmetic model presented by Majdi et al. (2012) as:

$$H_C = \frac{h_s(h_s + 3d)}{2d}. \tag{7}$$

The height of triangle  $A_iB_iC_i$  is calculated as:

$$h_{\Delta i} = [B_{Gi} + (2h_i \tan(45 - \varphi_p/2))] \tan \beta_i. \tag{8}$$

Considering GCM, the influence angle of CZ is calculated as:

$$\beta_i = \tan^{-1} \left( \frac{D_i G_i}{A_i G_i} \right), \tag{9}$$

where

$$D_1 G_1 = \left( \frac{H_c \sin \varphi_{01} - J_1 \sin(\varphi_{01} - \alpha)}{\sin \varphi_{01} \sin(\varphi_{01} - \alpha)} \right) \sin \varphi_{01}, \tag{10}$$

$$D_2 G_2 = \left( \frac{H_c \sin \varphi_{02} - J_2 \sin(\varphi_{02} + \alpha)}{\sin \varphi_{02} \sin(\varphi_{02} + \alpha)} \right) \sin \varphi_{02}, \tag{11}$$

$$\begin{aligned} A_i G_i &= A_i H_i + F_i H_i + F_i G_i \\ &= [B_{Gi} + h_i \tan(45 - \varphi_p/2)] + \left( \frac{J_i + D_i G_i}{\tan \varphi_{0i}} \right). \end{aligned} \tag{12}$$

Equations (10)–(12) show that the triangle height depends on the caving angle, which is determined from the following equations:

$$\varphi_{01} = \tan^{-1}\left(\frac{H_c}{W_1}\right) + \alpha, \tag{13}$$

$$\varphi_{02} = \left| \tan^{-1}\left(\frac{H_c}{W_2}\right) - \alpha \right|. \tag{14}$$

Hence, the area of triangle  $A_iB_iC_i$  is calculated as follows:

$$S_{\Delta i} = \left[ \frac{B_{Gi} + h_i \tan(45 - \varphi_p/2)}{2} \right] h_{\Delta i}. \tag{15}$$

Within the triangle, because of damaged rock mass, resistance properties as well as EDZ are decreased. Therefore, the area of non-subscription, between the parabolic area of EDZ and the triangle  $A_iB_iC_i$ , is related to the additional loading on gate roadways (the area of the extended part of EDZ). Based on Fig. 3, the area of the extended part of EDZ can be calculated through integration. Functions  $f_1'(x)$ ,  $f_1''(x)$ ,  $f_2'(x)$ , and  $f_2''(x)$  are as follows:

$$f_1'(x) = \frac{h_{\Delta 1}}{2a_1}x, \tag{16}$$

$$f_2'(x) = -\frac{h_{\Delta 2}}{2a_2}x + h_{\Delta 2}, \tag{17}$$

$$f_1''(x) = f_2''(x) = -\frac{B_{ni}}{a_i^2}x^2 + \frac{2B_{ni}}{a_i}x, \tag{18}$$

where

$$a_i = \frac{B_{Gi} + h_i \tan(45 - \varphi_p/2)}{2}. \tag{19}$$

Therefore, the integral form of the area of the extended part of EDZ can be written as follows:

$$S_{\text{add1}} = \int_{x'_1}^{x''_1} [f_1'(x) - f_1''(x)] dx = \int_{x'_1}^{x''_1} \left[ \frac{h_{\Delta 1}}{2a_1}x - \frac{B_{n1}}{a_1^2}x^2 + \frac{2B_{n1}}{a_1}x \right] dx, \tag{20}$$

$$S_{\text{add2}} = \int_0^{x'_2} [f_2'(x) - f_2''(x)] dx = \int_0^{x'_2} \left[ -\frac{h_{\Delta 2}}{2a_2}x + h_{\Delta 2} - \frac{B_{n2}}{a_2^2}x^2 + \frac{2B_{n2}}{a_2}x \right] dx, \tag{21}$$

where,  $x'_1$ ,  $x'_2$ ,  $x''_1$ , and  $x''_2$  are:

$$f_1'(x) = f_1''(x) \Rightarrow \frac{h_{\Delta 1}}{2a_1}x_1 = -\frac{B_{n1}}{a_1^2}x_1^2 + \frac{2B_{n1}}{a_1}x_1 \Rightarrow \begin{cases} x'_1 = \frac{(4B_{n1} - h_{\Delta 1})a_1}{2B_{n1}}, \\ x''_1 = 2a_1 \end{cases}, \tag{22}$$

$$f_2'(x) = f_2''(x) \Rightarrow -\frac{h_{\Delta 2}}{2a_2}x_2 + h_{\Delta 2} = -\frac{B_{n2}}{a_2^2}x_2^2 + \frac{2B_{n2}}{a_2}x_2 \Rightarrow \begin{cases} x'_2 = \frac{h_{\Delta 2}a_2}{2B_{n2}}. \\ x''_2 = 2a_2 \end{cases}. \tag{23}$$

Hence, the area of the extended part of EDZ for the main gate and tail gate roadways can be obtained from:

$$S_{\text{add},i} = \frac{1}{48} \frac{a_i h_{\Delta i}^2 (12B_{ni} - h_{\Delta i})}{B_{ni}^2}. \tag{24}$$

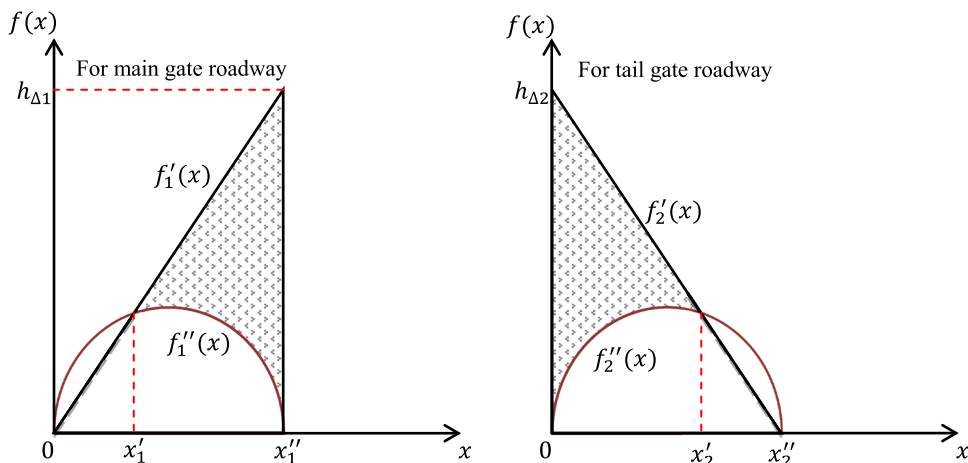
The area of extended EDZ (total area of EDZ) is calculated as:

$$S_{\text{ext},i} = S_{\text{par},i} + S_{\text{add},i}, \tag{25}$$

where the parabolic area of EDZ is obtained from the following equation (Mohammadi et al. 2013):

$$S_{\text{par},i} = \frac{2}{3} [B_{Gi} + h_i \tan(45 - \varphi_p/2)] B_{ni}. \tag{26}$$

**Fig. 3** The area for the extended part of EDZ due to longwall face effect



Moreover, considering the area of extended EDZ and Eq. (26), the height of the extended EDZ ( $B_{ni,ext}$ ) is calculated as:

$$B_{ni,ext} = \frac{3S_{ext,i}}{2[B_{Gi} + h_i \tan(45 - \varphi_p/2)]}. \quad (27)$$

Considering  $B_{ni} = B_{ni,ext}$  and Eq. (4), the equivalent height of overburden ( $H_{E,i}$ ) is determined from Eq. (28) and the total roof displacement due to the extended EDZ ( $u_{i,ext}$ ) can be calculated by setting  $H_i = H_{E,i}$  in Eq. (3):

$$H_{E,i} = \frac{\sigma_{cm}}{0.03} \ln \left( \left( \frac{3S_{ext,i}}{4B_{Gi}[B_{Gi} + h_i \tan(45 - \varphi_p/2)]} \right)^{1.67} + 1 \right). \quad (28)$$

Equation (27) shows the height of extended EDZ above a gate roadway at depth of  $H_i$ , which is under the face effect. Characteristics of the extended EDZ could be the same as those of EDZ for a gate roadway at depth  $H_{E,i}$  without any face effect on the gate roadway. Therefore, the concept of difference between  $H_i$  and  $H_{E,i}$  is used for calculating the face influence coefficient ( $FIC_i$ ) as in Eq. (29). It should be noted that, when there is no influence from longwall face on the gate roadway,  $FIC_i$  is equal to 1:

$$FIC_i = \frac{H_{E,i}}{H_i}. \quad (29)$$

#### 4 Computational Algorithm of Stability Analysis

As mentioned earlier, in stability analysis of gate roadways, two factors must be considered: (a) loading effect due to EDZ without the face effect and (b) loading effect due to extended EDZ considering the face effect. Pillar width plays a key role in transmission of load. It is important that the size of the pillar width is economical. To obtain an optimum design, a computational algorithm is presented for analyzing the gate roadway stability and design with optimum size for pillar width based on GCM (Fig. 4). This algorithm consists of five main stages as follows:

Stage 1: Without considering the face effect, the stability condition for the gate roadway is analyzed and the support system is designed.

Stage 2: After calculating the CZ height, the possibility of face effect on the gate roadway is investigated. If there is no effect, the design is finished; otherwise, we proceed to the next stage.

Stage 3: Considering the face effect, all characteristics of the extended EDZ are calculated.

Stage 4: Considering the characteristics of extended EDZ, the stability condition of the gate roadway is investigated. If the gate roadway is stable, the design is finished; otherwise, we proceed to the next stage. In this stage, the stability analysis is done considering an initial value of pillar width. To find the initial value, a suitable value for safety factor ( $S \cdot F_i$ ) is considered and the initial value of pillar width is determined by the following equation:

$$S \cdot F_i = \frac{\sigma_{P,i}}{\sigma_i}, \quad (30)$$

where  $\sigma_{P,i}$  and  $\sigma_i$  are the pillar strength and the average pillar stress, respectively (Hartman 1992).  $\sigma_{P,i}$  for a square or rectangular pillar can be determined based on Table 1.

Also, the following equations are used to calculate the average pillar stress (Whittaker and Singh 1981).

At a square pillar considering sub-critical subsidence condition:

$$\sigma_i = \frac{9.81\gamma}{1000W_i^2} \left( (L + W_i) \cdot H_i - \frac{L^2 \cot \varphi_i}{4} \right) W_i \text{ for } \frac{L}{H_i} < 2 \tan \varphi_i. \quad (31)$$

For a square pillar considering critical and supercritical mining subsidence conditions:

$$\sigma_i = \frac{9.81\gamma}{1000W_i^2} (W_i H_i + H_i^2 \tan \varphi_i) W_i \text{ for } \frac{L}{H_i} \geq 2 \tan \varphi_i, \quad (32)$$

where  $\phi_i$  is the average angle of shear of roof strata.

Also, the average pillar stress at a rectangular pillar is calculated as follows.

For sub-critical subsidence condition:

$$\sigma_i = \frac{9.81\gamma}{1000W_i L_i} \left( (L + W_i) \cdot H_i - \frac{L^2 \cot \varphi_i}{4} \right) L_i \text{ for } \frac{L}{H_i} < 2 \tan \varphi_i. \quad (33)$$

For critical and supercritical mining subsidence conditions:

$$\sigma_i = \frac{9.81\gamma}{1000W_i L_i} (W_i H_i + H_i^2 \tan \varphi_i) L_i \text{ for } \frac{L}{H_i} \geq 2 \tan \varphi_i, \quad (34)$$

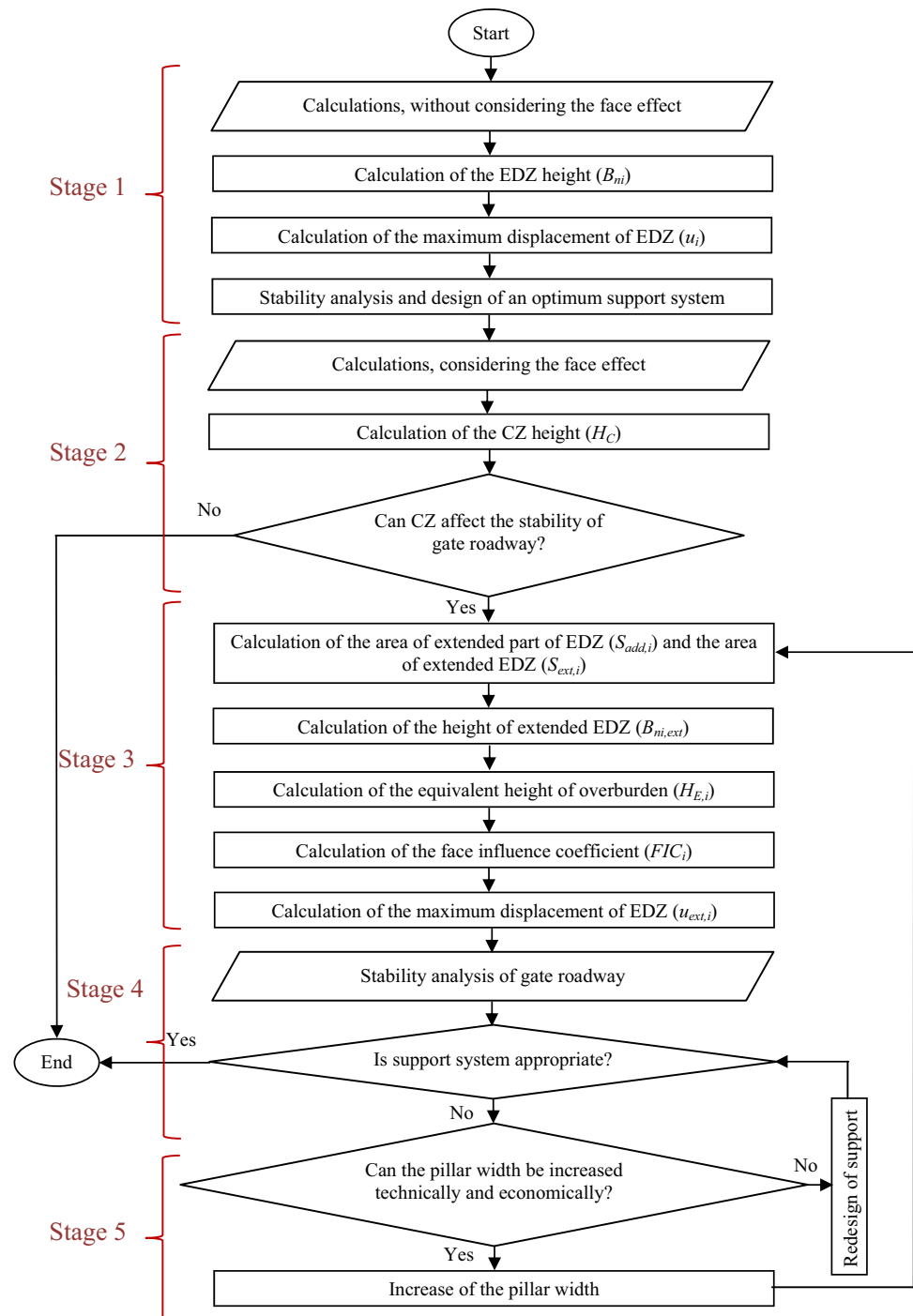
where  $L_i$  is the pillar length.

The pillar length is normally determined based on the ventilation requirements and operations. It is equal to or greater than the pillar width (Hartman 1992).

Stage 5: As GCM models a cross section of face behind the advance longwall mining, the role of pillar width in transition of the addition loading due to CZ to the gate roadways is more important than the role of length pillar. On the other hand, as shown in Table 1, the pillar strength for square and rectangular pillars is a function of



**Fig. 4** Computational algorithm for optimum pillar design based on GCM



pillar width and pillar height (pillar height and face height are the same). Hence, three solutions are suggested for stabilizing the gate roadway: (1) increasing pillar width, (2) increasing bearing capacity of the support system, and (3) increasing pillar width and bearing capacity of the support system simultaneously. It should be noted that for selecting each solution and achieving an optimum design, technical and economical feasibility factors must be considered.

## 5 Validation of GCM

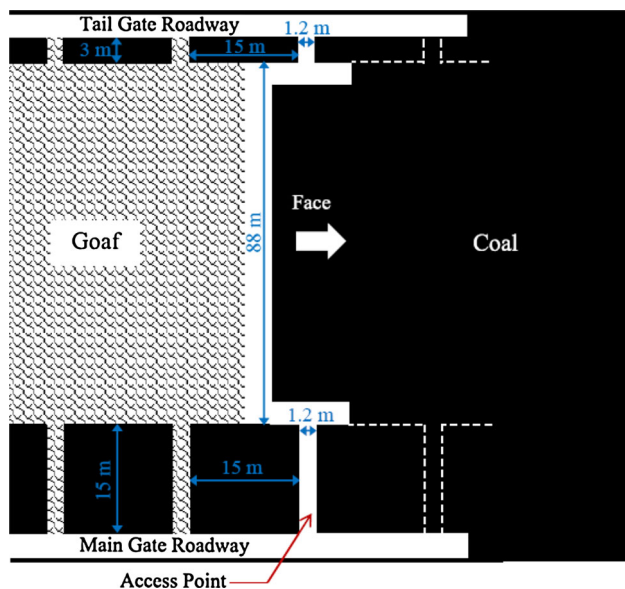
To validate the performance of GCM in determining the characteristics of extended EDZ above the main gate and tail gate roadways, one of the conventional (non-mechanized) advance longwall faces of Parvade-2 coal mine of Tabas, Iran, was considered. The Parvade-2 coal mine, with an area of about 40 km<sup>2</sup> and total reserve of about 5 million tons, is one of five coal areas of Tabas consisting of

**Table 1** Some empirical equations for calculating the pillar strength

Equation	Explanation	References
$\sigma_{P,i} = \sigma_c \sqrt{\frac{W_i}{h_{P,i}}}$	$\sigma_c$ is the uniaxial compressive strength of a cubical specimen and $h_{P,i}$ is the pillar height	Holland (1964)
$\sigma_{P,i} = \sigma_c \left( 0.778 + 0.222 \frac{W_i}{h_{P,i}} \right)$	–	Obert and Duvall (1967)
$\sigma_{P,i} = 7.2 \frac{W_i^{0.46}}{h_{P,i}^{0.66}}$	In Australia, a coefficient of 7.4 is used	Salamon and Munro (1967)
$\sigma_{P,i} = \sigma_c \left( 0.64 + 0.36 \frac{W_i}{h_{P,i}} \right)$	–	Bieniawski (1968)
$\sigma_{P,i} = \sigma_c \exp \left( -0.43 + 0.668 \sqrt{\frac{W_i}{h_{P,i}}} \right)$	–	Oraei et al. (2009a)

three coal seams, B<sub>1</sub>, B<sub>2</sub>, and C<sub>1</sub>, in which C<sub>1</sub> and B<sub>2</sub> have high extraction possibility. Coal seam B<sub>2</sub> is extracted by advance longwall mining. The thickness of B<sub>2</sub>, including 37 % of mine reserve (1,500,000 ton), varies from 0.4 to 1.75 m. Hanging wall of B<sub>2</sub> consists of siltstone, sandy siltstone, and sandstone, and the footwall consists of argillite and sandstone (Javaheri 2009).

According to Fig. 5, the length of the face is 88 m and, to protect the main gate roadway and tail gate roadway, pillars with width 15 and 3 m are considered. The depths of the main and tail gate roadways are 120 and 64 m, respectively. Moreover, the width and height of both the gate roadways are 3.60 and 2.60 m, respectively. Due to high convergence in the supported main gate roadway, displacements of each gate roadway are measured using instrumentation and monitoring operations. The results show that the face effect on the main gate roadway is very high and the maximum convergence at the roof is about 45 cm,

**Fig. 5** Plan of a longwall face in Parvade-2 coal mine, Tabas

whereas for the tail gate roadway, due to the low face effect, the maximum roof displacement is about 9.5 cm (Javaheri 2009). Figure 6 shows the situation of main gate roadway after convergence. Also, a comparison of the main gate roadway before and after convergence is shown in Fig. 7.

According to Eq. (7), CZ height is equal to 15.2 m. Other characteristics of the longwall face are shown in Table 2. The main gate and tail gate roadways are analyzed using GCM along with the suggested algorithm, and the obtained results are presented in Tables 3 and 4.

As shown in Table 3, for the main gate roadway, face influence coefficient of 4.76 is obtained and the EDZ is extended about 219 %. Moreover, the roof displacement at  $q_1 = 60$  kPa, without considering the face effect, is 3.47 cm, whereas by considering the face effect, this displacement increased by about 1133 % to 42.78 cm. Also, according to Table 4, at the tail gate roadway, face influence coefficient is equal to 2.93 and extension of EDZ is about 103 %. Moreover, the roof displacement at

**Fig. 6** Main gate roadway in Parvade-2 coal mine after convergence





**Fig. 7** Comparison of main gate roadway situation before and after convergence in Parvade-2 coal mine

$q_2 = 60$  kPa is increased from 0.56 to 8.98 cm. Comparison of the obtained displacement with the measured displacement indicates that errors by GCM in calculating the roof displacements of the main gate and tail gate roadways are 5 and 6.5 %, respectively.

## 6 Discussion

To investigate the effects of (1) pillar width, (2) bearing capacity of support system, (3) simultaneous effects of pillar width and bearing capacity of support system, and (4)

coal seam dip on characteristics of extended EDZ, sensitivity analyses were carried out on the main gate roadway. Also, the effect of coal seam dip on roof displacements and the face influence coefficient were evaluated at the main gate and tail gate roadways.

### 6.1 The Effect of Pillar Width

GCM shows that the area of triangle  $A_iB_iC_i$  is a function of pillar width. To investigate the effect of pillar width in transferring the additional loads on the main gate roadway, a series of analyses were performed and parameters of area for extended EDZ, face influence coefficient, and roof displacement were evaluated as shown in Fig. 8. As seen from this figure, the relationships between pillar width and output parameters are nonlinear, and for small pillar width the output parameters increase rapidly.

Decreasing  $W_1$  from 15 to 10 m (decreasing by about 33 %) causes an extension of about 40 % in the area of EDZ, an increase of about 82 % in the roof displacement, and an increase of about 42 % in the face influence coefficient. However, on increasing  $W_1$  from 15 to 20 m (increasing by about 30 %), the roof displacement is decreased from 42.78 to 28.62 cm (decreasing by about 33 %) and the face influence coefficient is decreased from 4.76 to 3.67 (decreasing by about 23 %). Also, on increasing  $W_1$  by about 100 % (increasing from 15 to 30 m), the roof displacement is decreased by about 58 % (from 42.78 to 18.11 cm) and the face influence coefficient decreases by about 43 % (from 4.76 to 2.71).

**Table 2** Characteristics of a longwall face in Parvade-2 coal mine (Javaheri 2009)

$\gamma$ (t/m <sup>3</sup> )	$\alpha$ (°)	$\varphi_p$ (°)	$\sigma_{cm}$ (MPa)	$q_1$ (kPa)	$q_2$ (kPa)	$\varphi_r$ (°)	$c_r$ (MPa)	$K$	$d$	$J_1$ (m)	$J_2$ (m)
2.3	28	28	15	60	60	15	0.05	1.1	0.12	0	0

**Table 3** Modeling results for the main gate roadway based on GCM

$S_{par,1}$ (m <sup>2</sup> )	$B_{n1}$ (m)	$u_1$ (cm)	$\varphi_{01}$ (°)	$S_{\Delta 1}$ (m <sup>2</sup> )	$S_{add,1}$ (m <sup>2</sup> )	$S_{ext,1}$ (m <sup>2</sup> )	$B_{n1,ext}$ (m)	$H_{E,1}$ (m)	$u_{ext,1}$ (cm)	FIC <sub>1</sub>
12.86	2.87	3.47	73.38	4.05	28.19	41.05	9.16	570.72	42.78	4.76

**Table 4** Modeling results for the tail gate roadway based on GCM

$S_{par,2}$ (m <sup>2</sup> )	$B_{n2}$ (m)	$u_2$ (cm)	$\varphi_{02}$ (°)	$S_{\Delta 2}$ (m <sup>2</sup> )	$S_{add,2}$ (m <sup>2</sup> )	$S_{ext,2}$ (m <sup>2</sup> )	$B_{n2,ext}$ (m)	$H_{E,2}$ (m)	$u_{ext,2}$ (cm)	FIC <sub>2</sub>
9.09	2.03	0.56	50.84	18.17	9.42	18.51	4.13	205.30	8.98	2.93

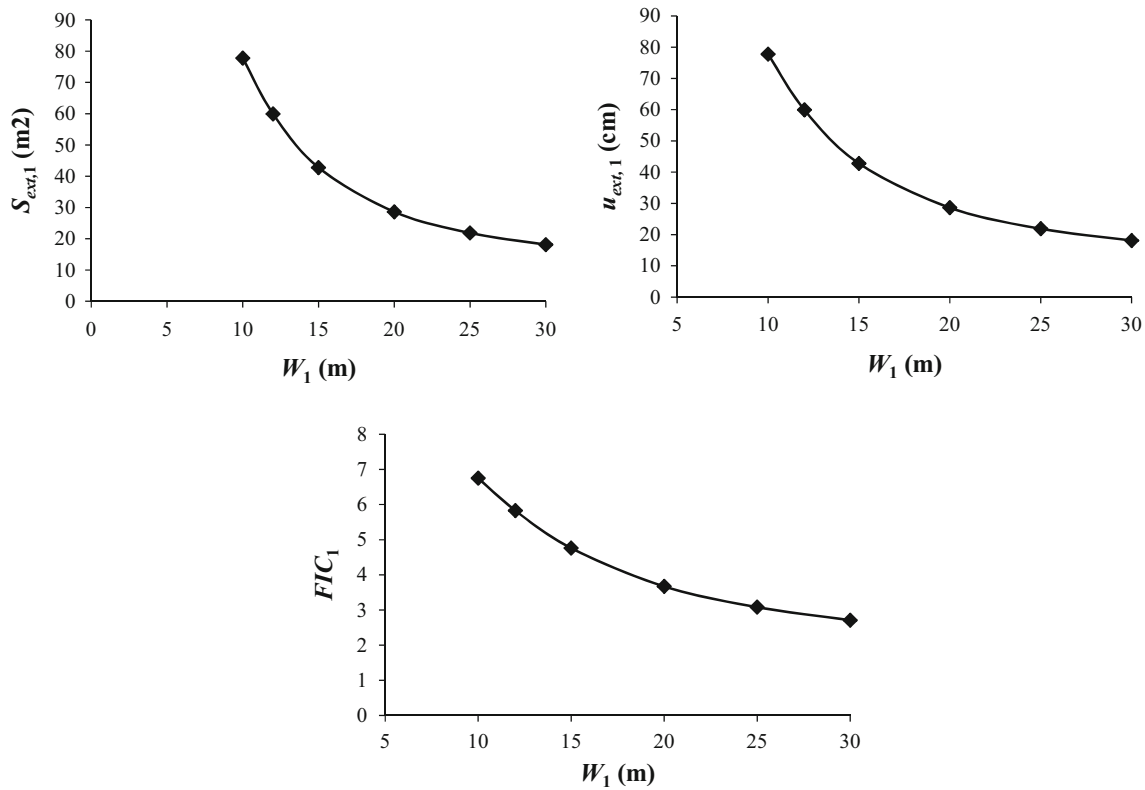


Fig. 8 Sensitivity analysis of pillar width effect on the main gate roadway stability at  $q_1 = 60$  kPa

### 6.2 The Effect of Bearing Capacity of the Support System

According to Eq. (3), the roof displacement depends on the bearing capacity of the support system. Thus, a sensitivity analysis of the bearing capacity of the support system effect on the roof displacement of extended EDZ is carried out. As shown in Fig. 9, increasing the bearing capacity does not influence the roof displacement greatly; increasing  $q_1$  from 60 to 250 kPa (increasing by about 317 %) causes a reduction of about 47 % in the roof displacement (the roof displacement decreases from 42.78 to 22.87 cm).

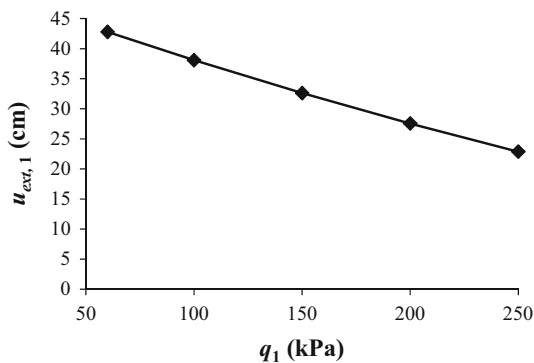


Fig. 9 Sensitivity analysis of bearing capacity of support effect on the roof displacement at  $W_1 = 15$  m

### 6.3 Simultaneous Effects of Pillar Width and Bearing Capacity of the Support System

Figures 8 and 9 show that increasing pillar width or bearing capacity of the support system alone may not be suitable for reducing the displacements of extended EDZ. Therefore, a sensitivity analysis was carried out for investigating the simultaneous effect of pillar width and bearing capacity of the support system on roof displacements (Fig. 10). As explained earlier in Sect. 6.1, at

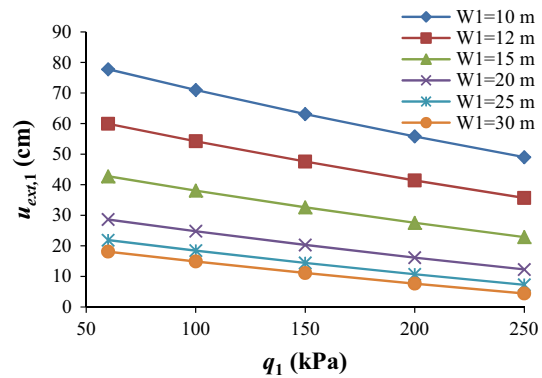
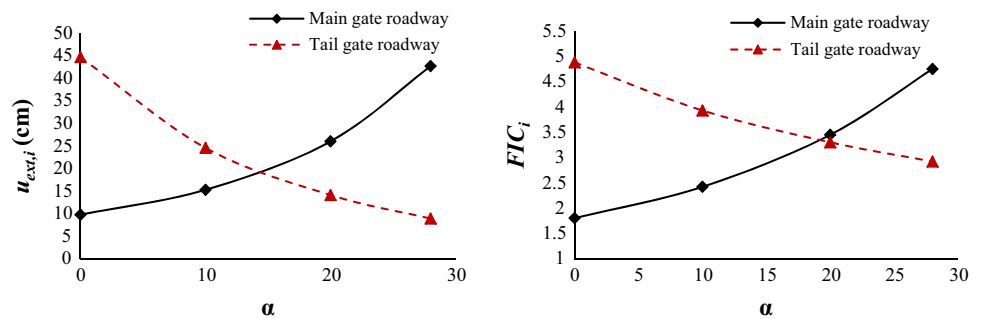


Fig. 10 Sensitivity analysis of the simultaneous effect of pillar width and bearing capacity of the support system on the roof displacements

**Fig. 11** Sensitivity analysis of the coal seam dip effect on stability of the main gate roadway at  $W_1 = 15$  m and  $q_1 = 60$  kPa and tail gate roadway at  $W_2 = 3$  m and  $q_2 = 60$  kPa



$q_1 = 60$  kPa, due to increase of  $W_1$  from 15 to 30 m, the roof displacements are decreased to 18.11 cm (decreasing by about 58 %). Also, according to Fig. 9, at  $W_1 = 15$  m, increasing  $q_1$  from 60 to 250 kPa causes a reduction of about 47 % and the roof displacement is equal to 22.87 cm. However, based on Fig. 10, on increasing  $q_1$  from 60 to 250 kPa and  $W_1$  from 15 to 30 m simultaneously, this reduction is about 90 % and the roof displacements are equal to 4.43 cm.

#### 6.4 The Effect of Coal Seam Dip

To investigate the effect of coal seam dip on the stability of the gate roadways,  $\alpha = 0^\circ, 10^\circ, 20^\circ$ , and,  $28^\circ$  were considered and the resulting roof displacement of extended EDZ and face influence coefficient are presented in Fig. 11. Results show that the effect of  $\alpha$  on output parameters is very significant; decreasing  $\alpha$  from  $28^\circ$  to  $0^\circ$  causes a reduction of about 77 % in  $u_{ext,1}$  and 62 % in  $FIC_1$  at the main gate roadway and an increase of about 398 % in  $u_{ext,2}$  and 67 % in  $FIC_2$  at the tail gate roadway.

Obviously, when the coal seam dip is zero and  $W_1$  is equal to  $W_2$ , the face effect on the main gate and tail gate roadways should be the same. Hence, considering  $W_1 = W_2 = 15$  m and  $\alpha = 0^\circ$ , it is observed that the face has the same effect. Roof displacement and face influence coefficient at the main gate and tail gate roadways were obtained as 9.84 and 1.81 cm, respectively, which demonstrates that GCM has been designed with high accuracy.

## 7 Conclusions

In this paper, a new empirical method was presented for calculating the roof displacement and height of EDZ surrounding gate roadways. Also, a GCM was developed for calculating the face effect on the extension of EDZ at the main and tail gate roadways simultaneously. Unlike previous models, GCM considers the coal seam dip and the vertical distance between the coal pillar and roof of the gate roadway to determine the location of the coal seam at

the sidewall of the gate roadway. Moreover, a computational algorithm was presented for stability analysis of gate roadways and selection of the optimum pillar width for gate roadways. GCM was validated against field data from Parvade-2 coal mine in Tabas, Iran. The obtained results showed good performance of GCM, such that the errors from GCM for calculating the roof displacements of the main gate and tail gate roadways were 5 and 6.5 %, respectively. Furthermore, the results from sensitivity analyses show that simultaneous design of pillar and bearing capacity of the support system is the best solution method for control of roof displacements in EDZ. Finally, it was concluded that the effect of coal seam dip on the main gate and tail gate roadway stability was very significant.

**Acknowledgments** Grateful acknowledgment is made to Ali Javaheri and Hojat Darbani, Negin Coal Company of Tabas, Iran, who helped in obtaining data from instrumentation and monitoring in Parvade-2 coal mine of Tabas.

## References

- Bieniawski ZT (1968) The effects of specimen size on the compressive strength of coal. *Int J Rock Mech Min Sci* 5:325–335
- Biron C, Arioglu E (1983) *Design of support in mines*. Wiley, USA
- Chang SH, Lee CI, Lee YK (2007) An experimental damage model and its application to the evaluation of the excavation damage zone. *Rock Mech Rock Eng* 40(3):245–285
- Chuen LT (1979) Practice and knowledge of coal mining under water bodies. 10th World Mining Congress, Istanbul
- Fawcett RJ, Hibberd S, Singh RN (1986) Analytic calculations of hydraulic conductivities above longwall coal face. *Int J Mine Water* 45–60
- Gao F, Stead D, Kang H, Wu Y (2014a) Discrete element modelling of deformation and damage of a roadway driven along an unstable goaf—a case study. *Int J Coal Geol* 127:100–110
- Gao F, Stead D, Coggan J (2014b) Evaluation of coal longwall caving characteristics using an innovative UDEC Trigon approach. *Comput Geotech* 55:448–460
- Hartman HL (1992) *SME Mining engineering handbook*, 2nd edn, vol 1. Society for Mining, Metallurgy, and Exploration, Inc, USA
- Hoek E (1998) Tunnel support in weak rock. Keynote address Symp on sedimentary rock engineering, Taiwan, pp 20–22
- Holland CT (1964) The strength of coal in mine pillars. In: *Proceedings of the sixth symposium on rock mechanics*, pp 450–456

- Horyl P, Marsalek P (2014) Load-bearing capacity of frictional joints in steel arch yielding supports. In: 22nd SVSFEM ANSYS Users' Group Meeting and Conference, pp 49–56
- Janas P (1990) Dimensioning of roadway supports in conditions of Ostrava-Karvina coalfield. In: Proceedings of World Mining Congress, Novosibirsk, pp 124–129
- Janas P, Snuparek R, Krejsa M (2009) Probabilistic approach to designing anchor support in mine workings in Ostrava-Karvina coal district. *Tunel* 4:37–43
- Javaheri A (2009) Stress analysis around a lateral gallery; case study: level III, Parvade-2 coal mine-Tabas. M Eng thesis, Shahid Bahonar University of Kerman, Iran
- Jiao YT, Song L, Wang XZ, Adoko AC (2013) Improvement of the U-shaped steel sets for supporting the roadways in loose thick coal seam. *Int J Rock Mech Min Sci* 60:19–25
- Jukes SG (1985) Study of deformation behaviour of steel arches in gate roadways. *Min Sci Technol* 3:63–80
- Lawrence W (2009) A method for the design of longwall gate road roof support. *Int J Rock Mech Min Sci* 46:789–795
- Lin H, Zhang B (2011) Study of soft rock roadway support technique. *Procedia Eng* 26:321–326
- Majdi A, Hassani FP, Yousef Nasiri M (2012) Prediction of the height of distressed zone above the mined panel roof in longwall coal mining. *Int J Coal Geol* 98:62–72
- Mohammadi H, Jalalifar H, Ebrahimi MA (2013) Prediction of damaged zone in longwall working roadways. Australian Coal Operators' Conference, Australia, pp 60–67
- Obert L, Duvall WI (1967) Rock mechanics and the design of structures in rocks. Wiley, New York
- Oraee K, Hosseini N, Gholinejad M (2009a) coal pillar strength based on the ground reaction curve—a new approach. In: Proceedings of the 28th international conference on ground control in mining, pp 21–24
- Pariseau WG (2007) Design analysis in rock mechanics. Taylor and Francis, London
- Peng S, Chiang H (1984) Longwall mining. Wiley, New York
- Pusch R, Stanfors R (1992) The zone of disturbance around blasted tunnels at depth. *Int J Rock Mech Min Sci Abstr* 29(5):447–456
- RafiqulIslam MD, Hayashi D, Kamruzzaman ABM (2009) Finite element modeling of stress distributions and problems for multi-slice longwall mining in Bangladesh, with special reference to the Barapukuria coal mine. *Int J Coal Geol* 78(2):91–109
- Salamon MDG, Munro AH (1967) A study of the strength of coal pillars. *J S Afr Inst Min Metall* 68:55–67
- Shen B, Poulsen B, Kelly M, Nemcik J, Hanson C (2003) Roadway span stability in tick seam mining-field monitoring and numerical investigation at Moranbah North mine. Australian Coal Operators' Conference, Australia, pp 173–184
- Singh MM, Kendorski FS (1981) Strata disturbance prediction for mining beneath surface water and waste impoundments. In: Proceedings of the 1st conference on ground control in mining, pp 76–89
- Snuparek R, Konecny P (2010) Stability of roadways in coalmines alias rock mechanics in practice. *J Rock Mech Geotech Eng* 2(3):281–288
- Suchowerska AM, Merifield RS, Carter JP, Clausen J (2012) Prediction of underground cavity roof collapse using the Hoek-Brown failure criterion. *Comput Geotech* 44:98–103
- Torano J, Rodriguez Diez R, Rivas Cid JM, Casal Barciella MM (2002) FEM modeling of roadways driven in a fractured rock mass under a longwall influence. *Comput Geotech* 29:411–431
- Unal E, Ozkan L, Cakmakci G (2001) Modeling the behavior of longwall coal mine gate roadways subjected to dynamic loading. *Int J Rock Mech Min Sci* 38:181–197
- Whittaker BN, Singh RN (1981) Stability of longwall mining gate roadways in relation to rib pillar size. *Int J Rock Mech Min Sci* 18:331–334
- Yavuz H (2004) An estimation method for cover pressure re-establishment distance and pressure distribution in the goaf of longwall coal mines. *Int J Rock Mech Min Sci* 41:193–205
- Zhou Y (1991) Evaluating the impact of multi-seam mining on recoverable coal reserves in an adjacent seam. Virginia Division of Mineral Resources, Commonwealth of Virginia, Department of Mines, Minerals and Energy, Pub Num:104